Electronic Supplementary Material (ESI) for Materials Chemistry Frontiers.

Supporting Information

NIR-triggered Engineering Photosynthetic Micro-Nanodevice for Reversing the Hypoxic Tumor Immunosuppressive Microenvironment

Mingming Guo, Shuang Li, Wenchang Peng, Shuchao Wang, Xiao-Dong Zhang, Tie Han, Bin Zheng, and Dong Ming**

Supplementary experimental section:

Reagents and Materials

Thulium(III) chloride hexahydrate ($TmCl_3 \cdot 6H_2O$), Ytterbium (III) chloride hexahydrate ($YbCl_3 \cdot 6H_2O$, 99.99%), Yttrium(III) chloride hexahydrate ($YCl_3 \cdot 6H_2O$, 99.99%), Octadecene (90%, technical grade), Ammonium fluoride (NH_4F, 99.99%), Oleic acid (90%, technical grade), NaOH, LPS, ICG, DOTAP, chloroplasts. YCl_3, $YbCl_3$ and $TmCl_3$ are from Shandong Jining TianYi Co., Ltd. Oleic acid is from Aladdin. LPS from Solarbio. ICG, DOTAP from Shanghai avet (A.V.T) Co., Ltd. Chloroplasts from spinach. Chloroplast Extraction Kit from Shanghai GuDuo Biotechnology Co., Ltd. Thermal imager from Changchun New Industry Iaser Co., Ltd.(Jilin).Fluorescence microscope from Nikon. Flow cytometry from BD. Apoptosis detection kit and DAPI are from Solarbio. The ROS testing kit from YIJI of Shanghai. Anoxia detection kit from YIJI of Shanghai. Healthy female C57BL/6 and BALB/c mice of 15-20 g body weight were purchased from HFK Technology Co., Ltd. (Beijing). Animal experiments were performed in accordance with the statutory requirements of People's Republic of China (GB14925-2010). Alanine aminotransferase (ALT) test kit, Aspartate aminotransferase (AST) test kit, Creatinine (Cre) test kit, Procalcitonin (PCT) test kit from Shanghai Enzyme-linked Biotechnology Co., Ltd.

Preparation of (LPS + ICG) @ DOTAP

The DOTAP was dissolved in dichloromethane and 2mL DOTAP (0.5mg/mL) was added to a round-bottom flask for spin steaming. After rotary steaming, put the round bottom flask into the oven, remove it after 12h, add 100 mL ICG (200 μg/mL) and 100 mL LPS (40 μg/mL) for ultrasound, and remove the solution after 6h of ultrasound, namely (LPS+ICG)@DOTAP.

Preparation of UCNs

Water solutions of YCl_3, $YbCl_3$ and $TmCl_3$ (molar concentration of 1 mol/L) were prepared, NaOH solution (molar concentration of 8 mol/L) was prepared, and NH_4F solution (2 mol/L) was prepared for standby. Measure 8mL NaOH solution and add it to a 250ml round bottom

flask. Add 25mL anhydrous ethanol and equal volume oleic acid while stirring. Stir for 10min and the mixture will become clear from turbidity. Add 20 mmol of rare earth element chloride solution (molar ratio Y^{3+}: Yb^{3+}: Tm^{3+}= 75/25/0.3) drop by drop, and continue stirring for 10 min. Take 5mL NH_4F solution and slowly add it to the round-bottom flask one drop at a time. Continue to stir for 30 min, and the solution was became a uniform liquid. Transfer the prepared mixed solution to two 50 mL hydrothermal kettles and place it in different high temperature ovens for reaction. The temperature was set at 180℃ and the time was 18h. After the reaction, turn off the power and cool down to room temperature naturally. Open the hydrothermal kettle had a distinct smell of oleic acid oxidized, the reaction solution was transparent light yellow brown, with white precipitate at the bottom. The products were centrifuged and washed repeatedly with ethanol and pure water for 3 times to remove the solvent. Pure up-conversion crystalline material was obtained.

Characterization of UCNs

High-resolution transmission electron microscopy (Tecnai G2 F20, FEI) was used to record the morphology and element mapping with an operating voltage of 200 kV. A fluorescence spectrophotometer (Cnilaser, China) was employed to measure the fluorescence spectrum of UCNs using 980 nm laser.

Chloroplasts extraction

Fresh spinach was prepared, cut into small pieces with clean scissors, quickly ground in a mortar, then filtered with gauze and centrifuged at 1000 rpm for 3min. The supernatant was taken and centrifuged at 3000 rpm for 5min. The chloroplasts were precipitated.

Chloroplasts oxygen production test

The oxygen production of chloroplasts was detected under blue light, purple light, white and yellow light. Irradiation for 30 seconds and stop for 30 seconds which was one cycle time (T)

and 21 cycle for each group. Chloroplasts oxygen production were detected at different pH, PBS was adjusted to different pH, and 21 cycle were irradiated with blue light. The chloroplasts and UCNs were irradiated with 21 cycle at 1:1 980 nm NIR.

Thermal imaging

The prepared 100 mL LID (100 μg/mL) was irradiated with 808 nm NIR and photographed every 10s. In animal thermal imaging, each mice was injected with 100 mL LID (100 μg/mL) and photographed successively every 10s.

Cell Culture

90% DMEM was mixed with 10% serum for cell culture. B16 cells were co-cultured with LID (10μg/mL) for 4 h and 3 min were irradiated continuously by 808 nm NIR. Dead and living cells were detected by AM/PI staining. The apoptotic cells were detected with the Apoptosis Detection Kit.

Mouse models and in vivo imaging

To develop the B16 tumor model for C57BL/6 mice and the 4T1 tumor model for BALB/c mice, 1×106 B16 cells (in 100μL of PBS) and 1×106 4T1 cells (in 100μL of PBS) were injected subcutaneously (s.c.) The treatment was carried out when the tumor growth reached 1 cm^3.

Experiments on animals

Subcutaneous injection of 50 μL LID (100 μg/mL) was given to the LID, LID+UCNs+cp, LID+UCNs+NIR, LID+cp+NIR and LID+UCNs+cp+NIR groups of C57BL/6 mice and the LID+UCNs+cp+NIR group of BALB/c mice. Subcutaneous injection of 50 μL PBS was given to mice of the PBS group of C57BL/6 mice and the PBS group of BALB/c mice the tumor was

irradiated with 808 nm NIR(2W) for 3min the next day. On the third day, subcutaneous injection of 50 μL fresh chloroplasts and UCNs (1:1) were given mice of the LID+UCNs+cp group. Subcutaneous injection of 50 μL UCNs was given mice of the LID+UCNs+NIR group. Subcutaneous injection of 50 μL fresh chloroplasts was given mice of the LID+cp+NIR group. Subcutaneous injection of 50 μL fresh chloroplasts and UCNs (1:1) were given mice of the LID+UCNs+cp+NIR group of C57BL/6 mice and the LID+UCNs+cp+NIR group of BALB/c mice. Give the LID+UCNs+NIR, LID+UCNs+cp+NIR and LID+UCNs+cp+NIR groups of C57BL/6 mice and the LID+UCNs+cp+NIR group of BALB/c mice of 980 nm NIR(2W) irradiation and 20 cycles were irradiated by 980 nm NIR. Weight and tumor size were measured daily. All the animal experiments involved in this work were approved by the Animal Ethics Committee of Tianjin University.

Hypoxia detection

The tumor was cut into 20 μm slices with a frozen sectioning machine for anoxic staining. Take pictures with a fluorescence microscope. Flow cytometry analysis: the tumor was ground, anoxia detection reagent was added, incubated at 4℃ for 30min, and detected by flow cytometry.

ROS detection

The tumor was cut into 20 μm slices with a frozen microtome for ROS staining. Take pictures with the fluorescence microscope. Quantitative detection: the tumor was ground, ROS detection reagent was added, and given at 37℃ for 1h.

Biological safety experiment

On day 0, mice were injected with LPS and LID subcutaneously, and their body temperature was measured with a thermometer for 7 consecutive days. Take blood from the eyes of the mice on the 1, 3, and 7 days after the injection, and take the serum for testing of ALT, AST, Cre, PCT.

Statistical Analyses

Each experiment group contained five repeated samples and data were expressed as mean ± standard deviation (SD) of experiments. Data analysis was performed using Origin 8.0. The significance between groups was analyzed using an unpaired two-tailed t test (comparing two groups) and one-way analysis of variance (ANOVA) (comparing multiple groups) by Statistics Analysis System (*$P < 0.05$, **$P < 0.01$ and ***$P < 0.001$, respectively). $P < 0.05$ was considered significant.

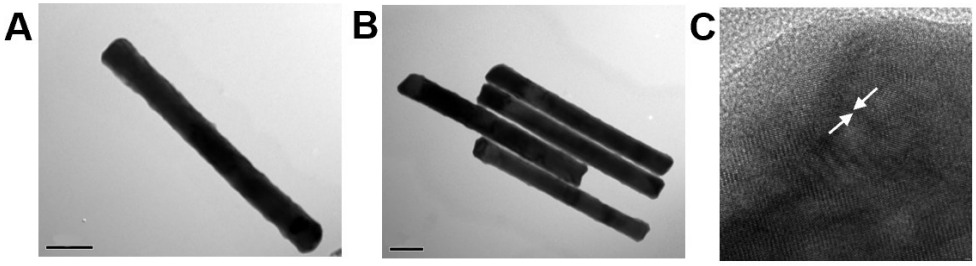

Fig. S1: A，B，C) TEM images of UCNs. A) Scale bars, 40 nm. B) Scale bars, 20 nm.

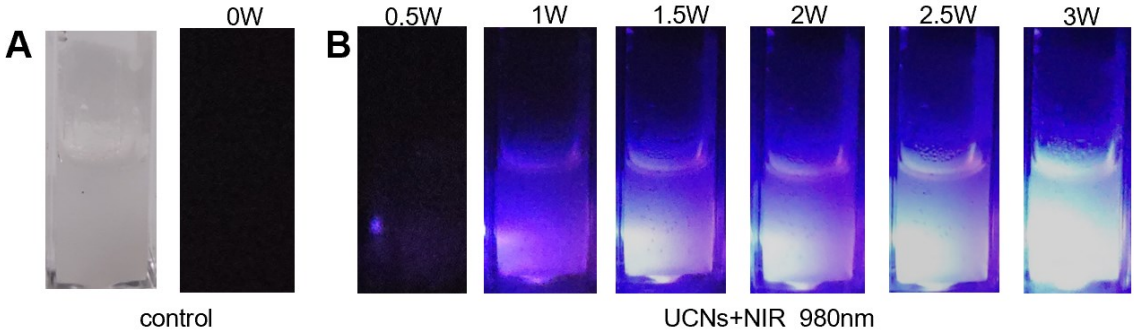

Fig. S2: UCNs were irradiated under 980 nm NIR at different power. A) The prepared UCNs were milky white. B) The luminescence of UCNs became stronger with the power of 980 nm NIR increased and the relationship between the two were proportional.

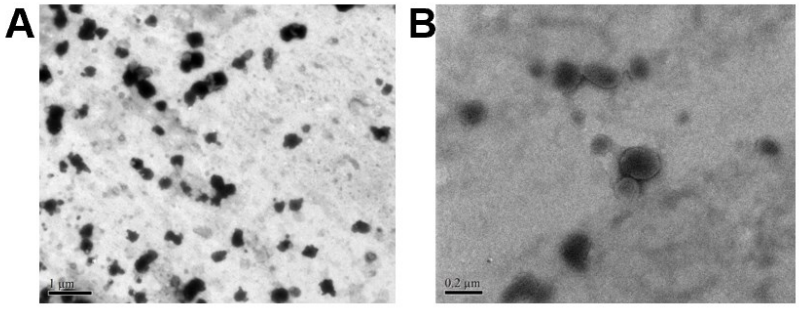

Fig. S3: Characterization of (LPS+ICG) @DOTAP. A, B) SEM images of (LPS+ICG) @DOTAP. A) Scale bars, 1μm. B) Scale bars, 200 nm.

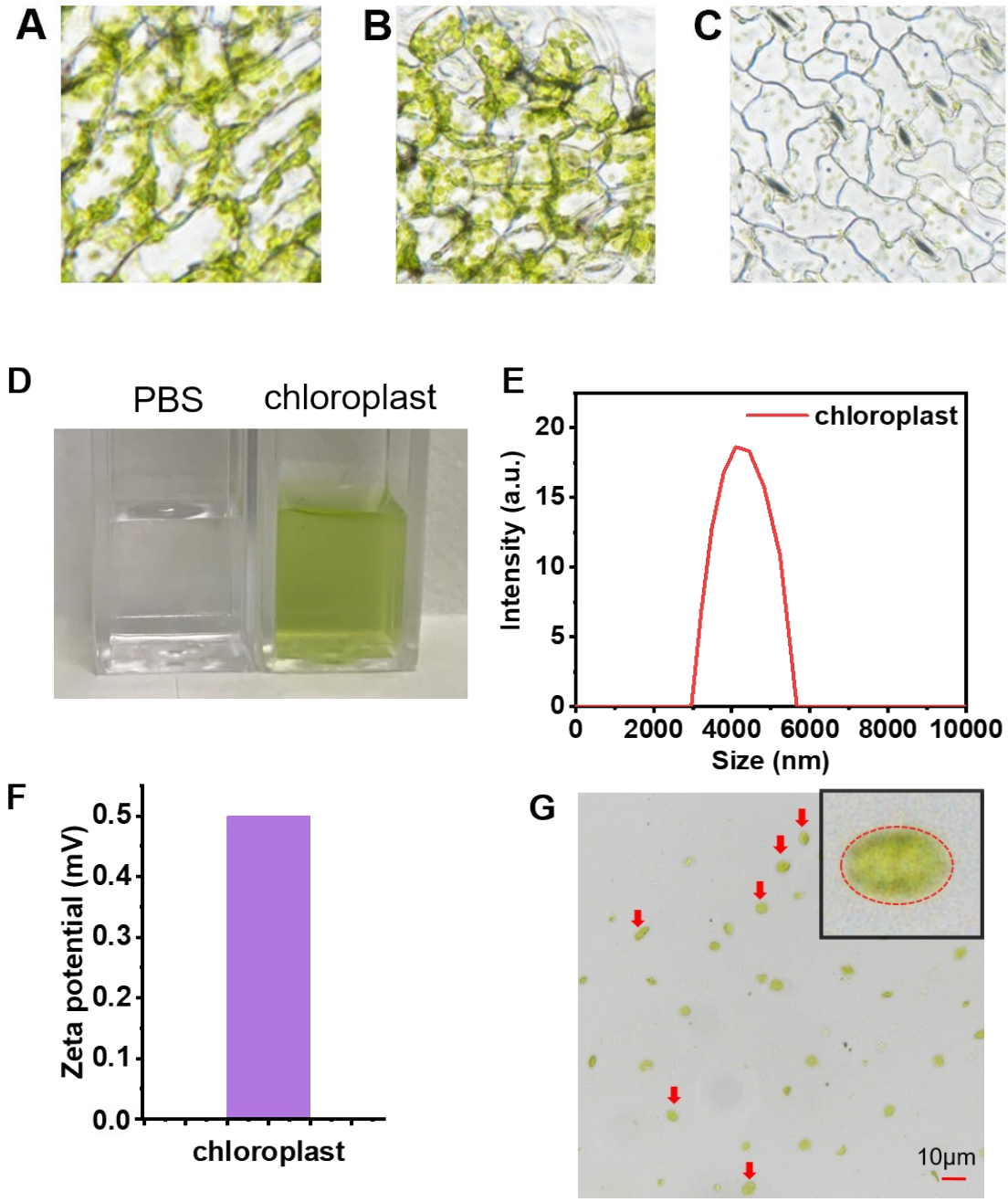

Fig. S4: A, B, C) The chloroplasts on the back of spinach were seen via the microscope. D) Image of chloroplasts. E) Chloroplast size. F) Zeta potential of chloroplast. G) Chloroplast morphology observed under a microscope. Scale bars, 10 μm.

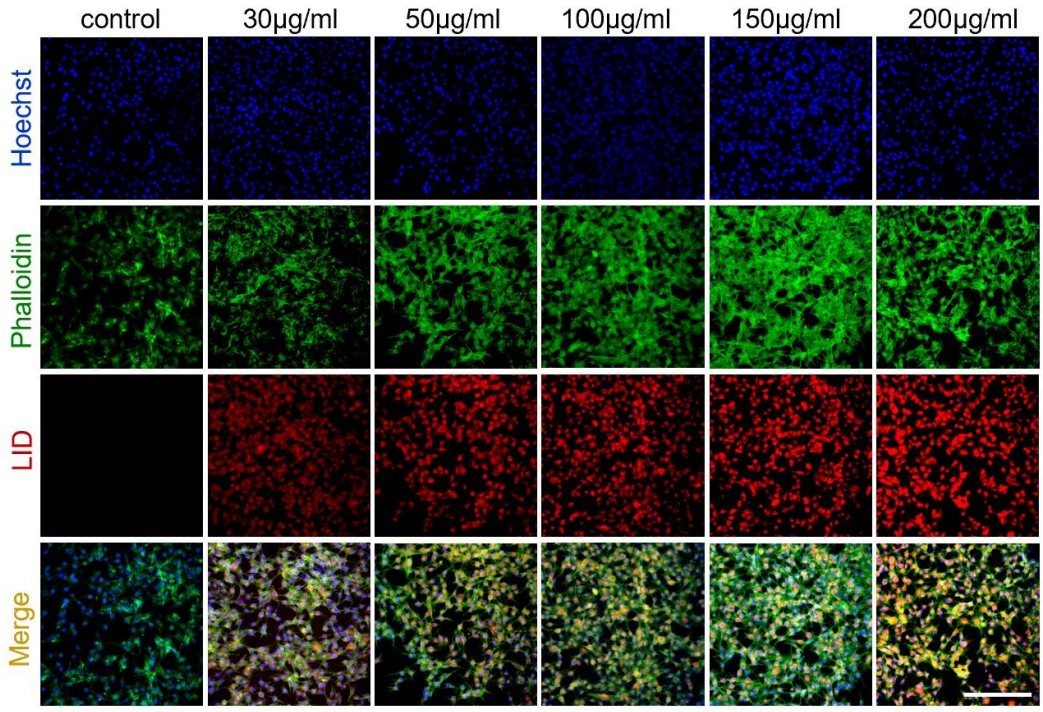

Fig. S5: To verify the morphology of B16 cells after LID endocytosis. Red was endocytosis LID, green was cytoplasm stained by phalloidin, and blue was nucleus stained by Hoechst. Scale bars, 100 μm.

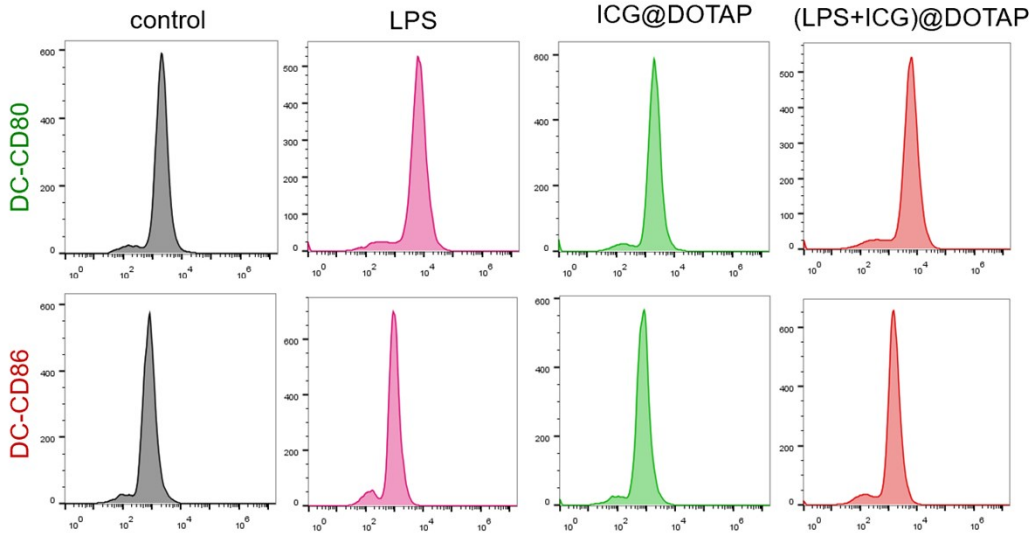

Fig. S6: Flow cytometry was used to verify the production of antibodies by LID activated DC 2.4 cells. Add LPS, ICG @DOTAP and (LPS+ ICG) @DOTAP to DC 2.4 cells, and LPS

activated DC 2.4 cells to produce CD80 and CD86. Add （LPS+ ICG）@DOTAP to achieve the same effect, while ICG @ DOTAP cannot stimulate DC 2.4 cells.

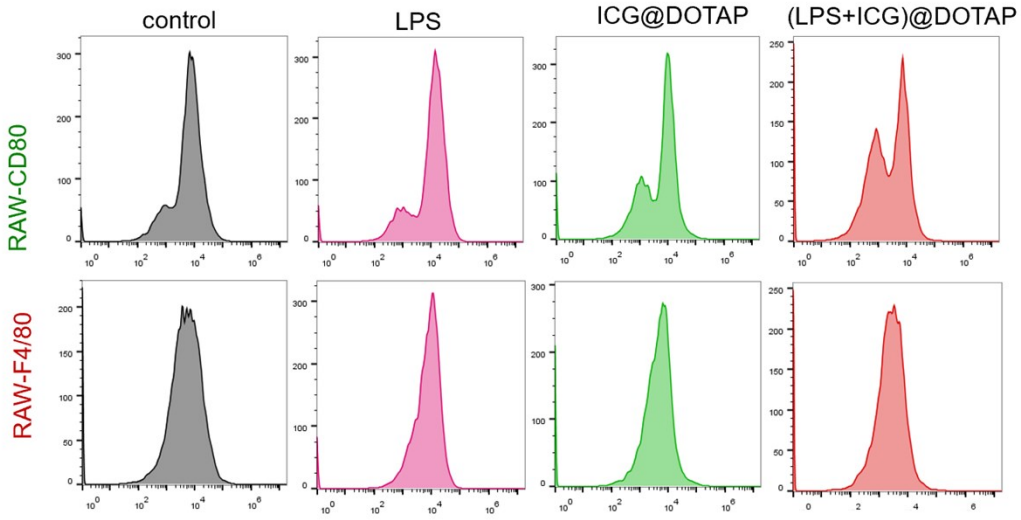

Fig. S7: Flow cytometry was used to verify the production of antibodies by LID activated RAW 264.7 cells.

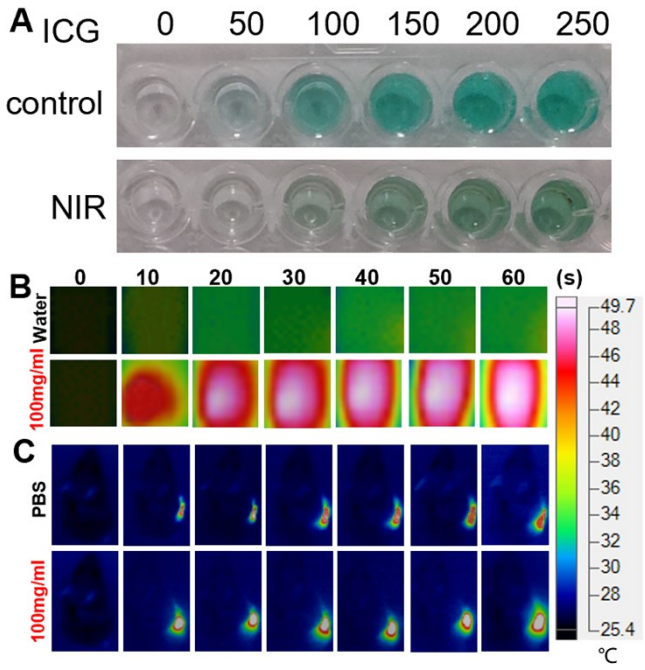

Fig. S8: A) ICG at different concentrations and it was irradiated via 808 nm NIR. B) LID photothermal effect in vitro. C) LID photothermal effect in vivo.

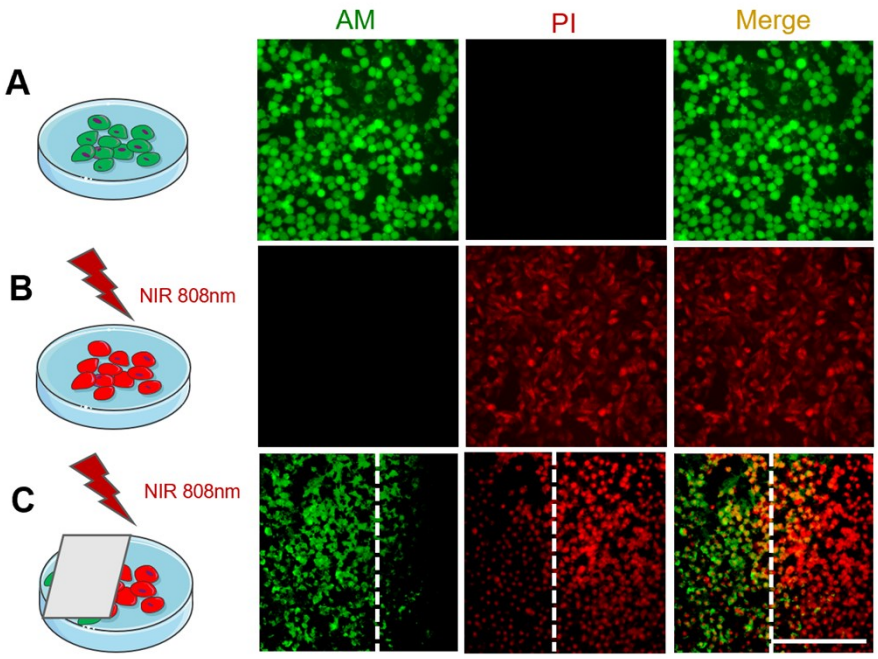

Fig. S9: Staining of dead cells and living cells. B16 and LID were mixed and cultured, irradiated with 808 nm NIR and stained with AM/PI. Active cells were dyed green by AM and dead cells were dyed red by PI. A) AM/PI staining of B16 cells. B) AM/PI staining via 808 nm NIR irradiation of B16 cells. C) Cover half of the cells with aluminum and stain with AM/PI via irradiation 808 nm NIR. Scale bars, 100 μm.

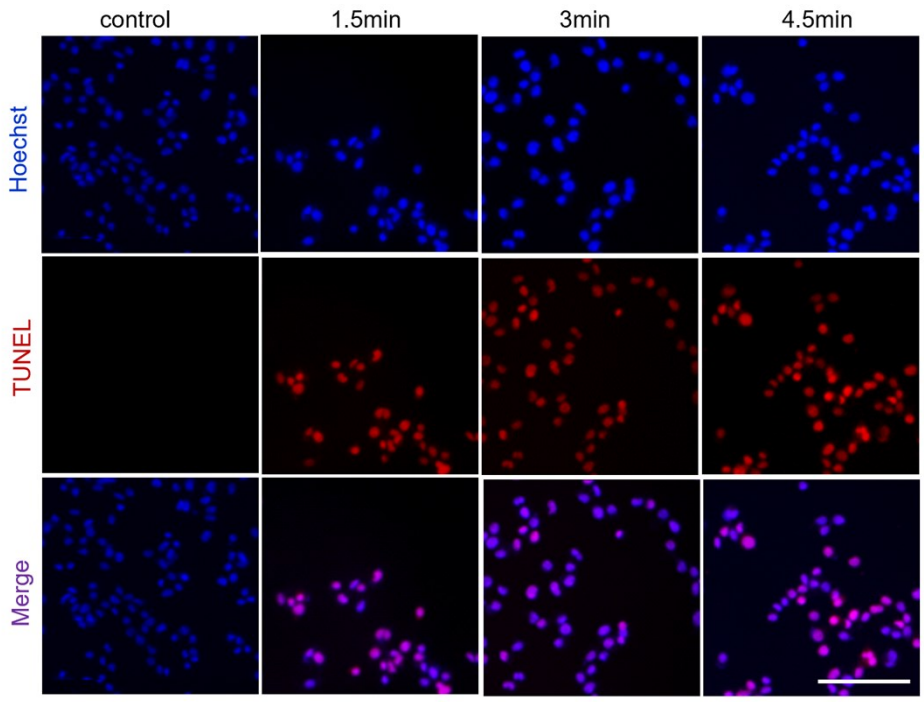

Fig. S10: TUNEL staining of B16 cells. The B16 cells co-cultured with LID were irradiated with 808 nm NIR for 1.5min, 3min and 4.5min, and the apoptotic cells were stained with TUNEL. Size bars, 100 μm.

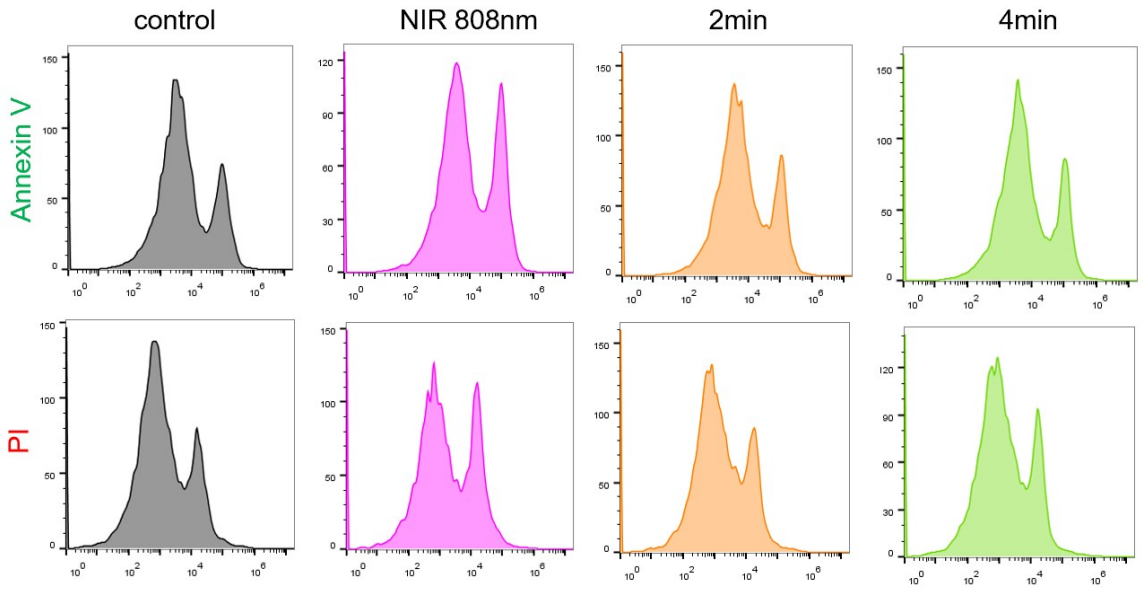

Fig. S11: The apoptotic cells were analyzed by flow cytometry. B16 cells co-cultured with LID were irradiated by 808 nm NIR, stained by Annexin V-FITC Apoptosis Detection Kit and analyzed by flow cytometry. Early apoptotic cells were stained with Annexin V and late apoptotic cells were stained with PI. After irradiation of 808 nm NIR for 2min and 4min, and the number of apoptotic cells increased significantly after irradiation with 808 nm NIR.

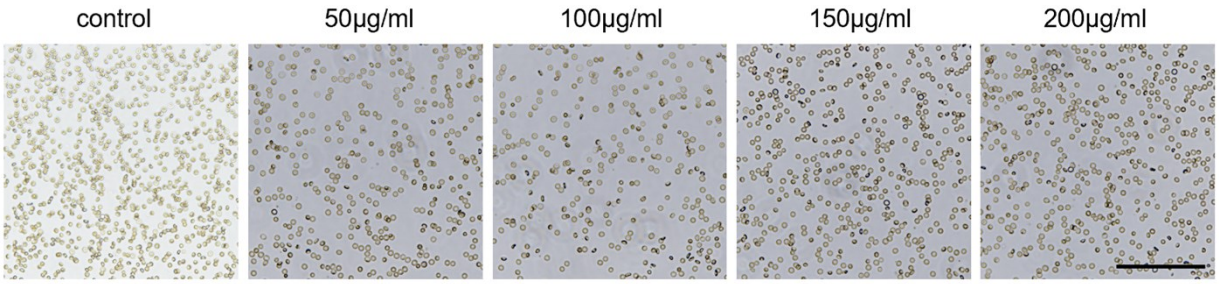

Fig. S12: Verify the security of LID. The morphology of blood cells after LID of different concentrations was added to the blood cells, LID had no effect on the morphology of blood cells, indicating that LID was non-toxic to cells and had higher safety. Scale bars, 200 μm.

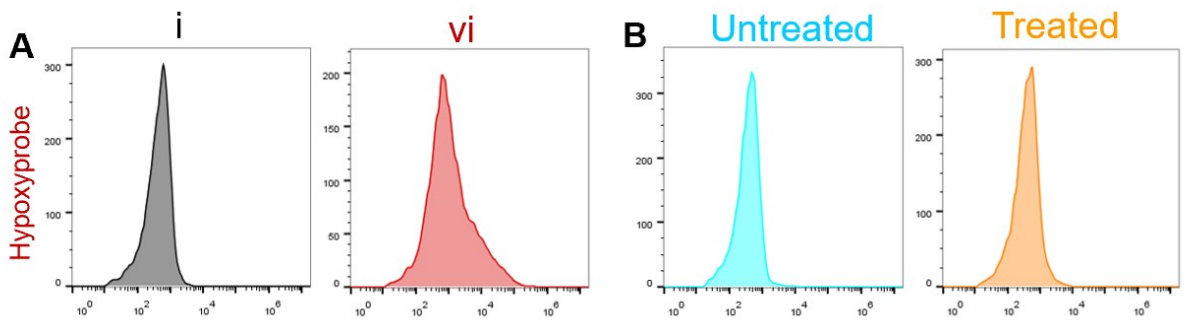

Fig. S13: Hypoxia was detected by flow cytometry. A) Flow cytometry was used to detect the changes of hypoxia in tumor of C57BL/6 mice after therapy of photosynthesis in vivo. B) Flow cytometry was used to detect the changes of hypoxia in tumor of BALB/c mice after therapy of engineering photosynthetic micro-nanodevice.

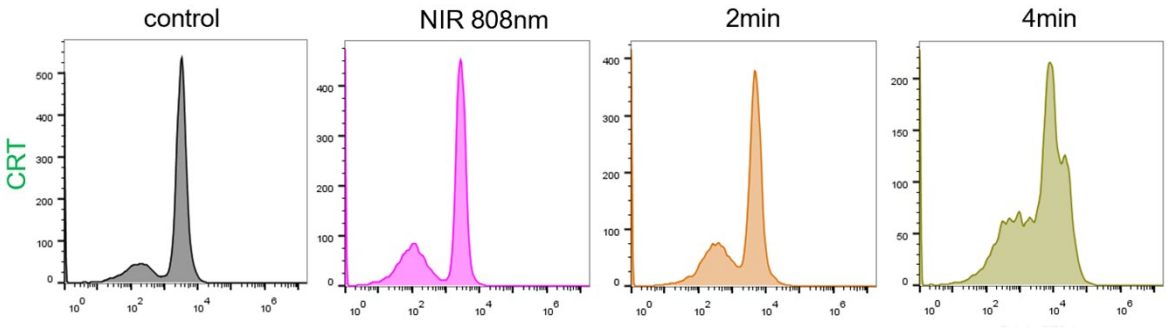

Fig. S14: CRT was analyzed by flow cytometry. The four groups were PBS, 808 nm NIR, after irradiation of 808 nm NIR for 2min and 4min.

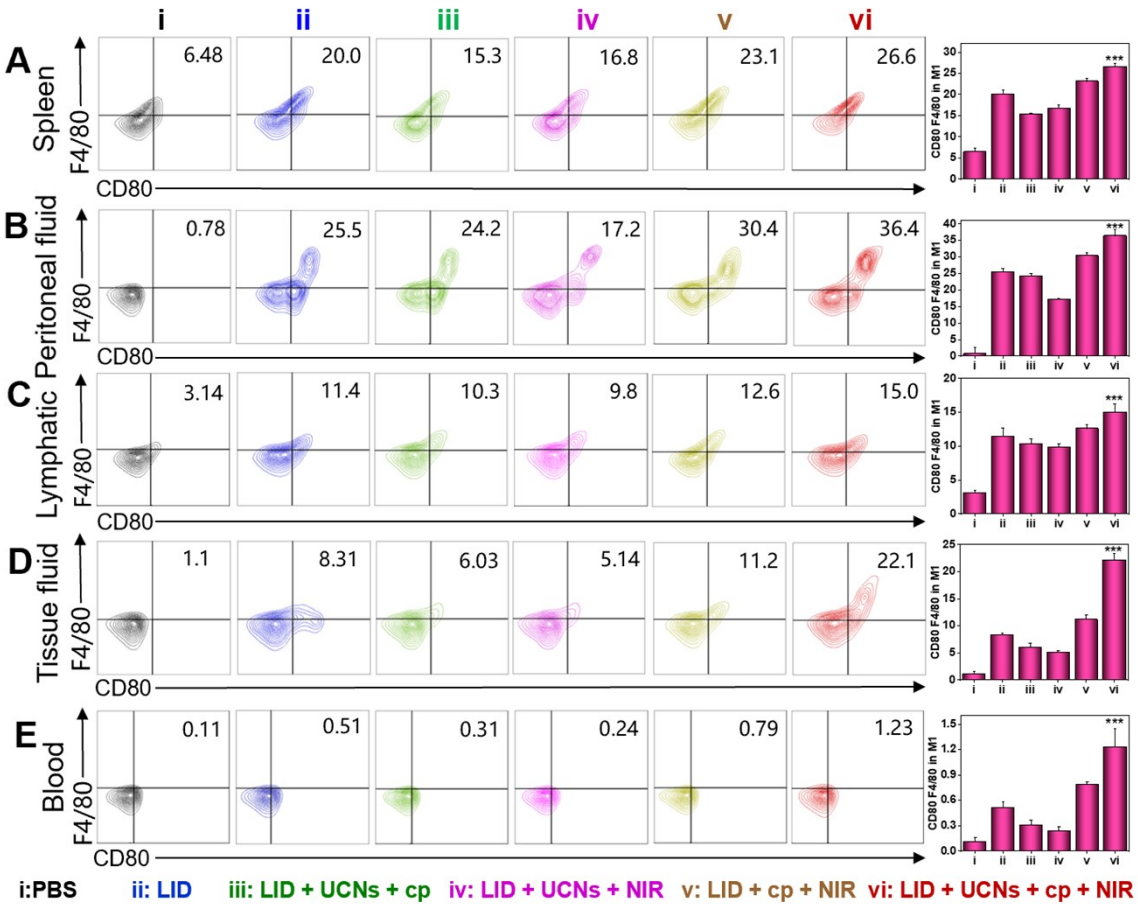

Fig. S15: Flow cytometry verified the number of M1 cells in different organs of C57BL/6 mice. After the injection of LID, M1 cells increased in all organs of mice, and the number of M1 cells was the largest after the operation of engineering photosynthetic micro-nanodevice. A) Spleen. B) Peritoneal fluid. C) Lymphatic. D)Tissue fluid. E) Blood. Data represent mean ± SD (n = 5); *P < 0.05, **P < 0.01 and ***P < 0.001 (one-way ANOVA).

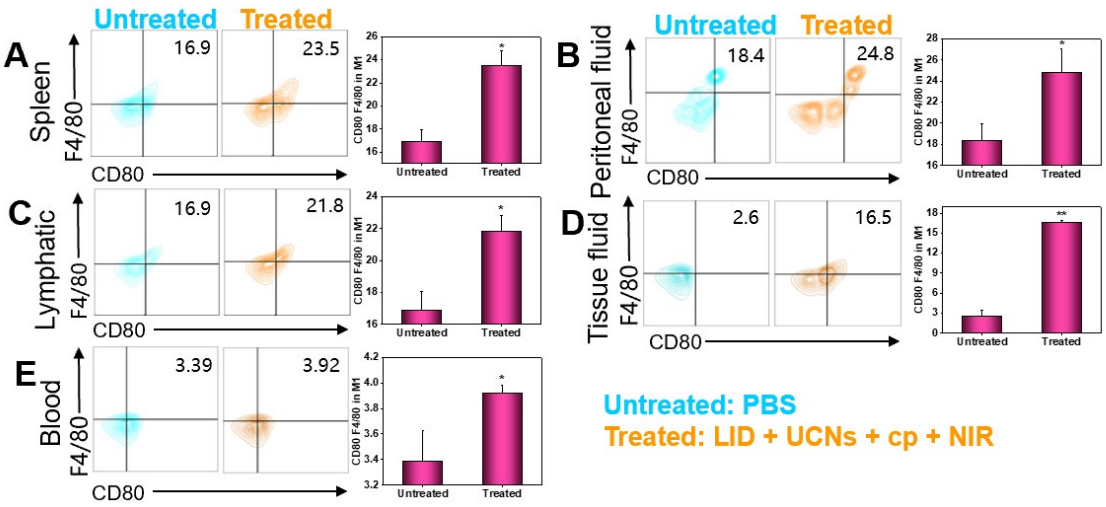

Fig. S16: Levels of M1 cells in different organs of BALB/c mice. The M1 cells content increased after engineering photosynthetic micro-nanodevice treatment. A) Spleen. B) Peritoneal fluid. C) Lymphatic. D) Tissue fluid. E) Blood. Data represent mean ± SD (n = 5); *P < 0.05, **P < 0.01 and ***P < 0.001 (one-way ANOVA).

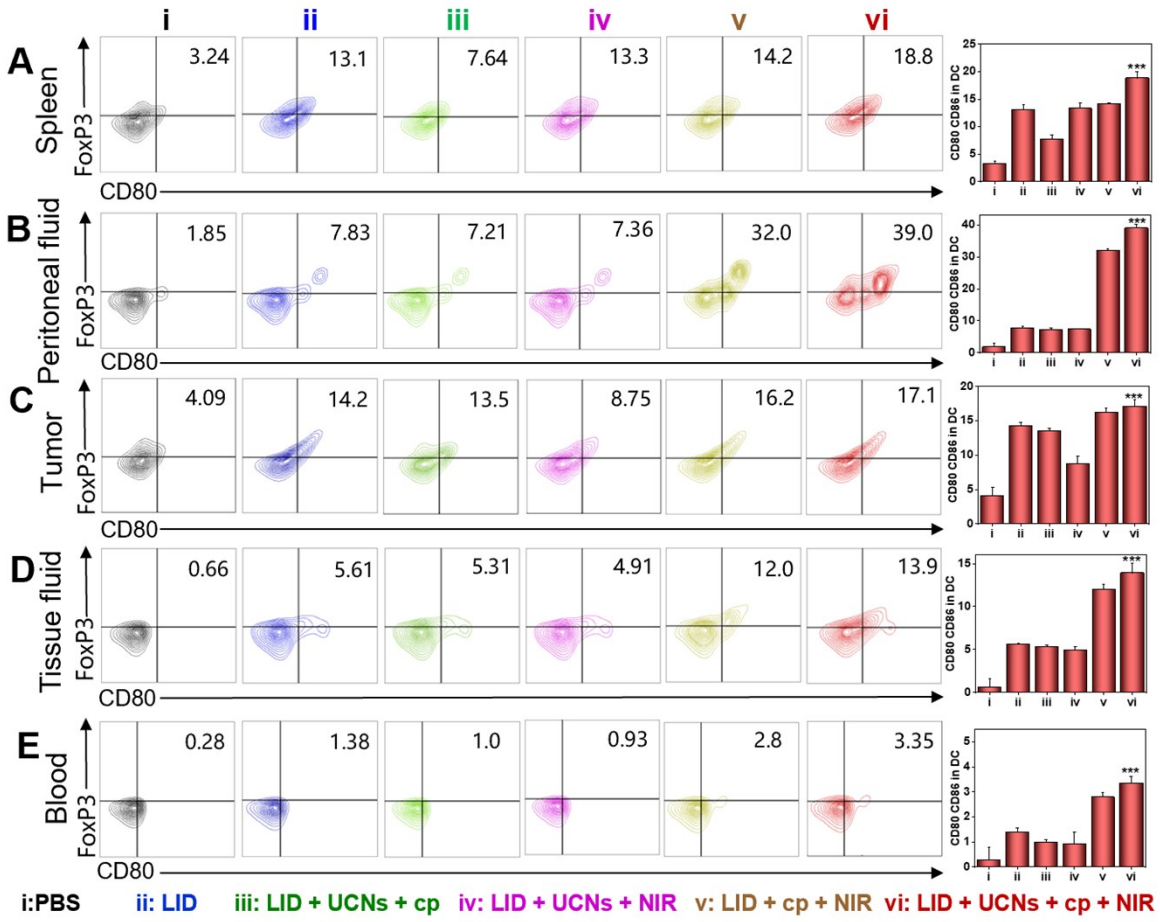

Fig. S17: Flow cytometry verified the number of DC cells in different organs of C57BL/6 mice, CD80 and CD86 labeled DC cells. After the injection of LID, DC cells increased in all organs of mice, and the number of DC cells was the largest after the operation of engineering photosynthetic micro-nanodevice. A) Spleen. B) Peritoneal fluid. C) Lymphatic. D) Tissue fluid. E) Blood. Data represent mean ± SD (n = 5); *P < 0.05, **P < 0.01 and ***P < 0.001 (one-way ANOVA).

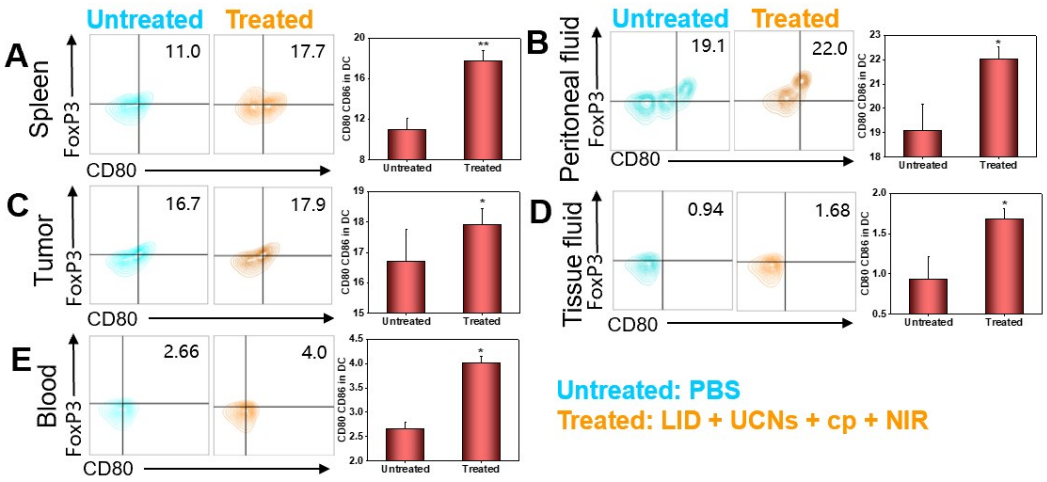

Fig. S18: Levels of DC cells in different organs of BALB/c mice, CD80 and CD86 labeled DC cells. The DC cells content increased after engineering photosynthetic micro-nanodevice treatment. A) Spleen. B) Peritoneal fluid. C) Lymphatic. D) Tissue fluid. E) Blood. Data represent mean ± SD (n = 5); *P < 0.05, **P < 0.01 and ***P < 0.001 (one-way ANOVA).

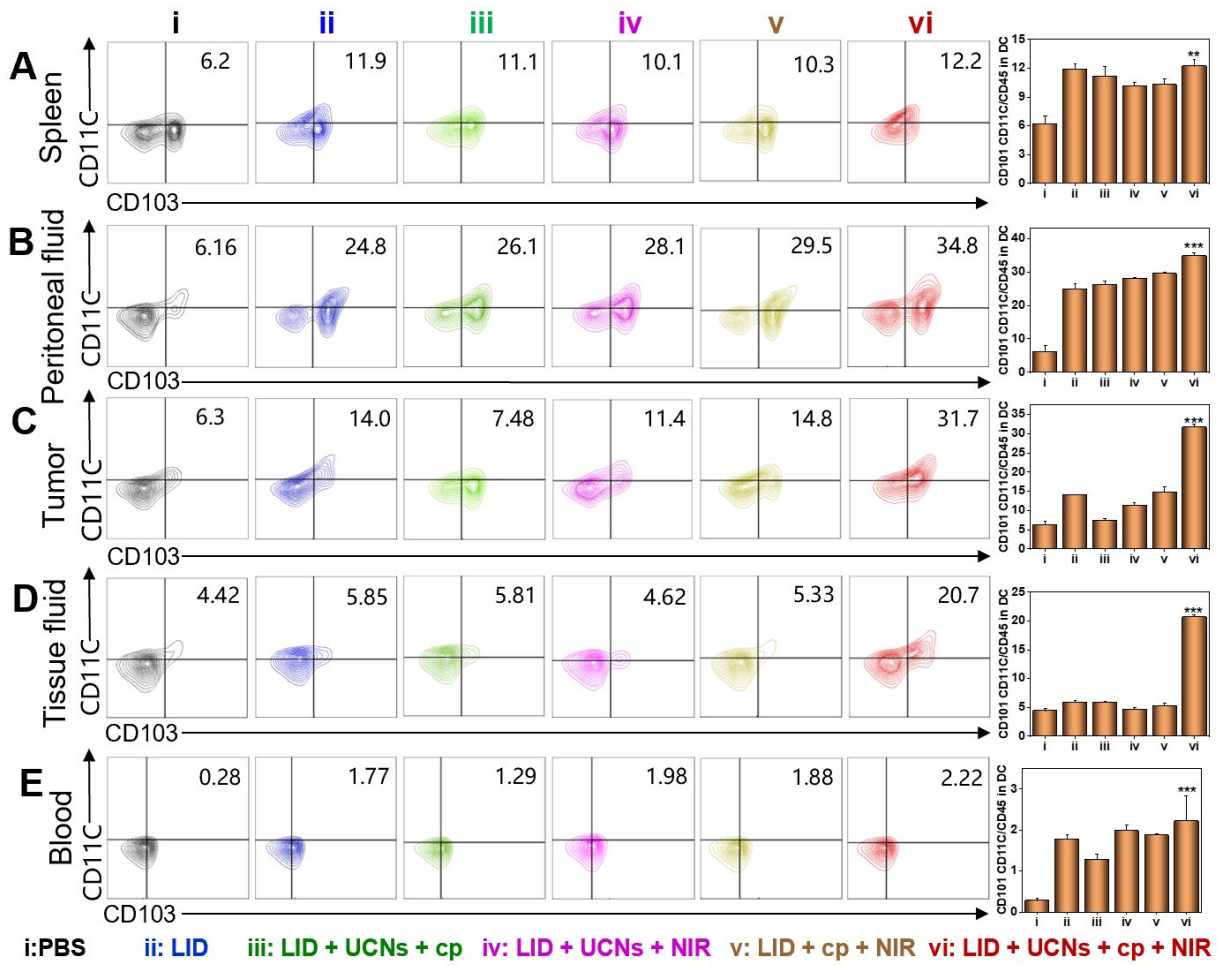

Fig. S19: Flow cytometry verified the number of DC cells in different organs of C57BL/6 mice, CD103 and CD11C labeled DC cells. After the injection of LID, DC cells increased in all organs of mice, and the number of DC cells was the largest after the operation of engineering photosynthetic micro-nanodevice. A) Spleen. B) Peritoneal fluid. C) Lymphatic. D) Tissue fluid. E) Blood. Data represent mean ± SD (n = 5); *P < 0.05, **P < 0.01 and ***P < 0.001 (one-way ANOVA).

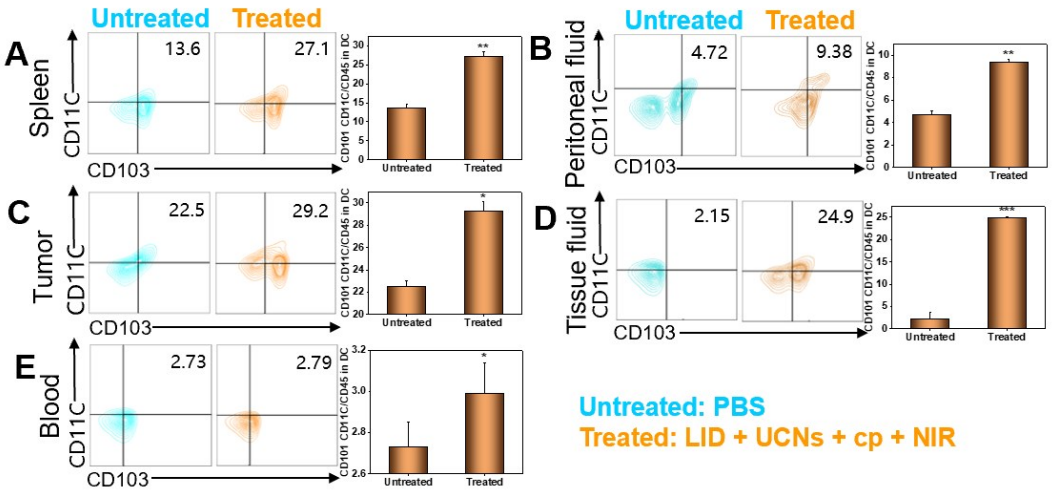

Fig. S20: Levels of DC cells in different organs of BALB/c mice, CD103 and CD11C labeled DC cells. The DC cells content increased after engineering photosynthetic micro-nanodevice treatment. A) Spleen. B) Peritoneal fluid. C) Lymphatic. D) Tissue fluid. E) Blood. Data represent mean ± SD (n = 5); *P < 0.05, **P < 0.01 and ***P < 0.001 (one-way ANOVA).

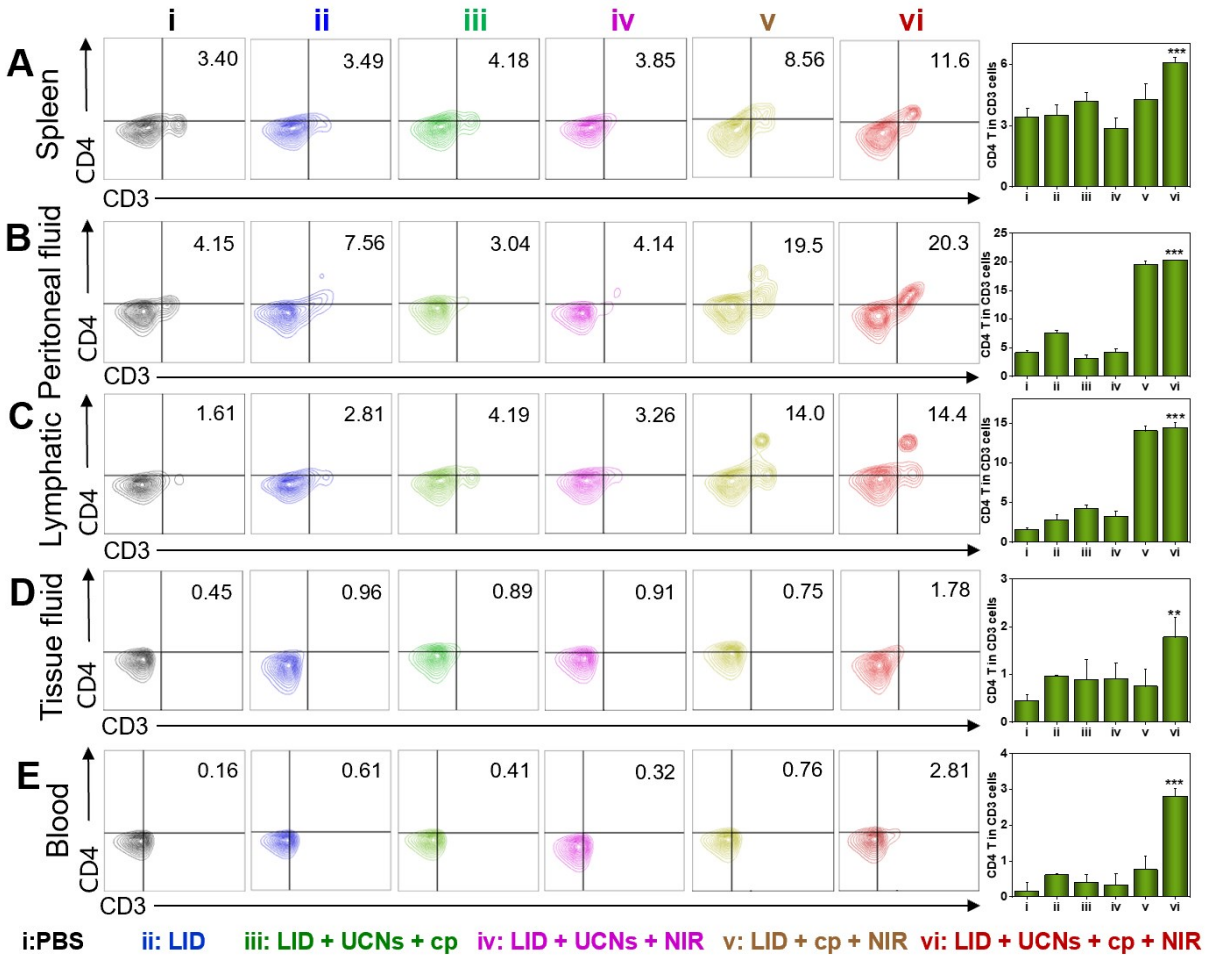

Fig. S21: Flow cytometry verified the number of $CD4^+$ T cells in different organs of C57BL/6 mice. After the injection of LID, $CD4^+$ T cells increased in all organs of mice, and the number of $CD4^+$ T cells was the largest after the operation of engineering photosynthetic micro-nanodevice. A) Spleen. B) Peritoneal fluid. C) Lymphatic. D) Tissue fluid. E) Blood. Data represent mean ± D (n = 5); *P < 0.05, **P < 0.01 and ***P < 0.001 (one-way ANOVA).

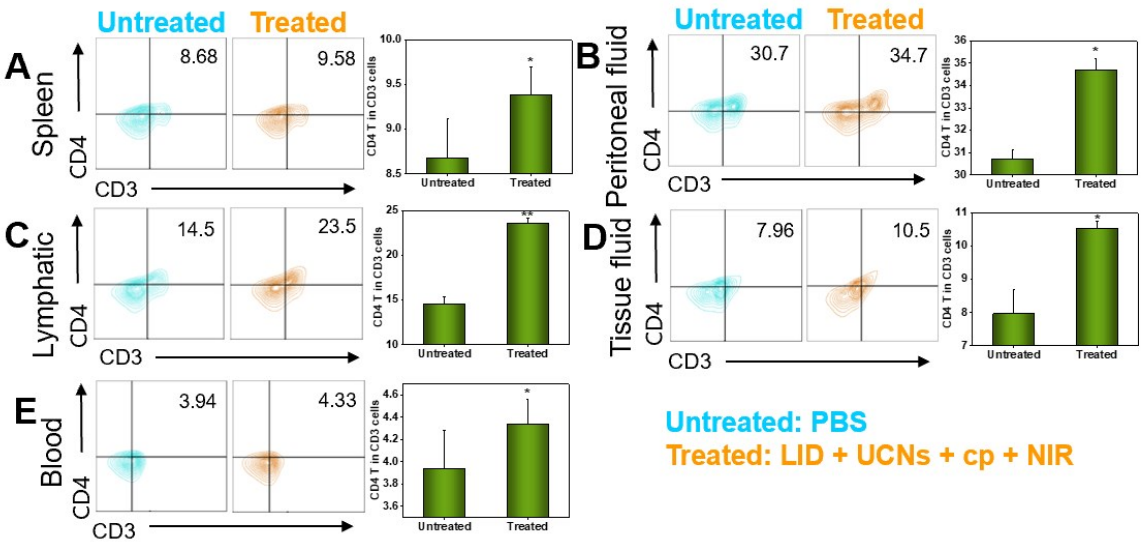

Fig. S22: Levels of $CD4^+$ T cells in different organs of BALB/c mice. The $CD4^+$ T cells content increased after engineering photosynthetic micro-nanodevice treatment. A) Spleen. B) Peritoneal fluid. C) Lymphatic. D) Tissue fluid. E) Blood. Data represent mean ± SD (n = 5); *P < 0.05, **P < 0.01 and ***P < 0.001 (one-way ANOVA).

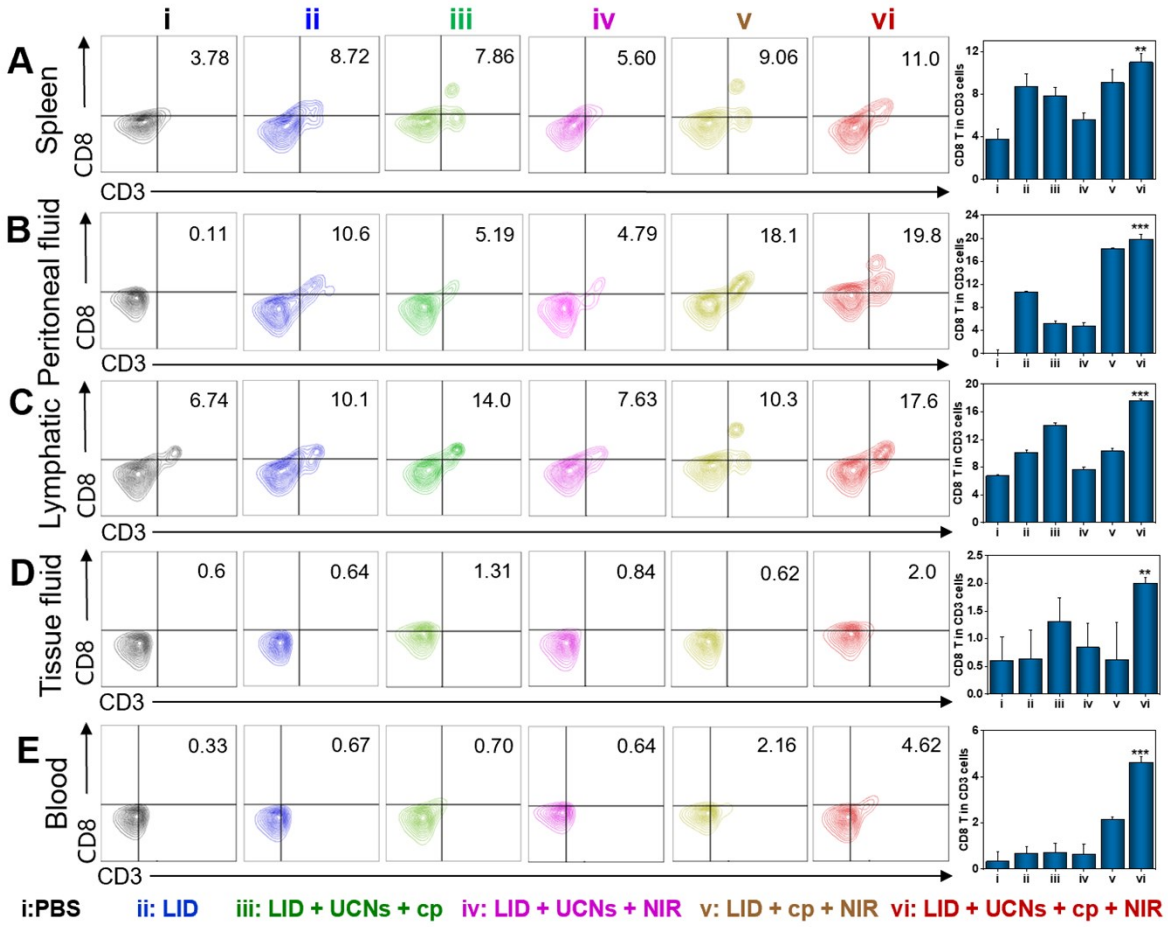

Fig. S23: Flow cytometry verified the number of $CD8^+$ T cells in different organs of C57BL/6 mice. After the injection of LID, $CD8^+$ T cells increased in all organs of mice, and the number of $CD8^+$ T cells was the largest after the operation of engineering photosynthetic micro-nanodevice. A) Spleen. B) Peritoneal fluid. C) Lymphatic. D) Tissue fluid. E) Blood. Data represent mean ± D (n = 5); *P < 0.05, **P < 0.01 and ***P < 0.001 (one-way ANOVA).

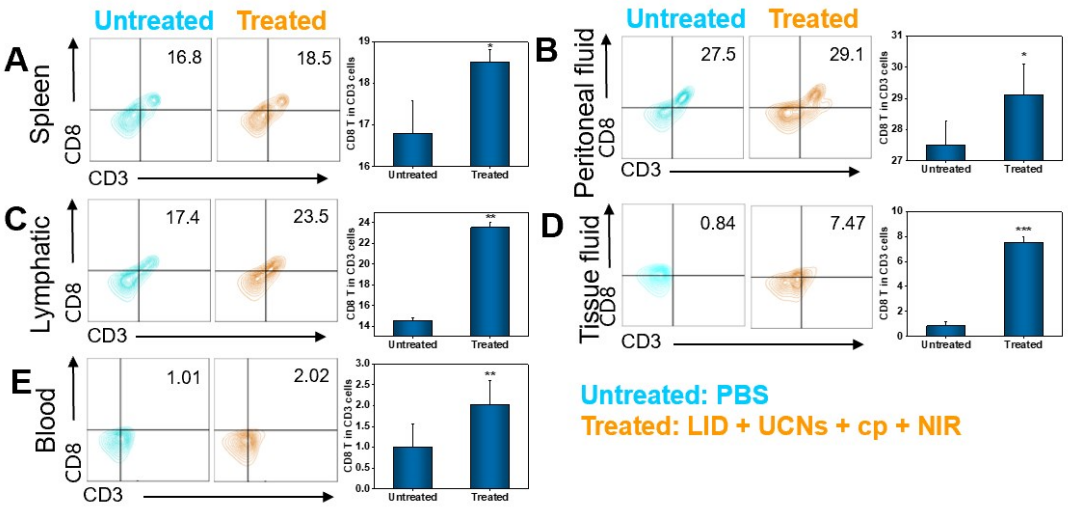

Fig. S24: Levels of $CD8^+$ T cells in different organs of BALB/c mice. The $CD8^+$ T cells content increased after engineering photosynthetic micro-nanodevice treatment. A) Spleen. B) Peritoneal fluid. C) Lymphatic. D) Tissue fluid. E) Blood. Data represent mean ± SD (n = 5); *P < 0.05, **P < 0.01 and ***P < 0.001 (one-way ANOVA).

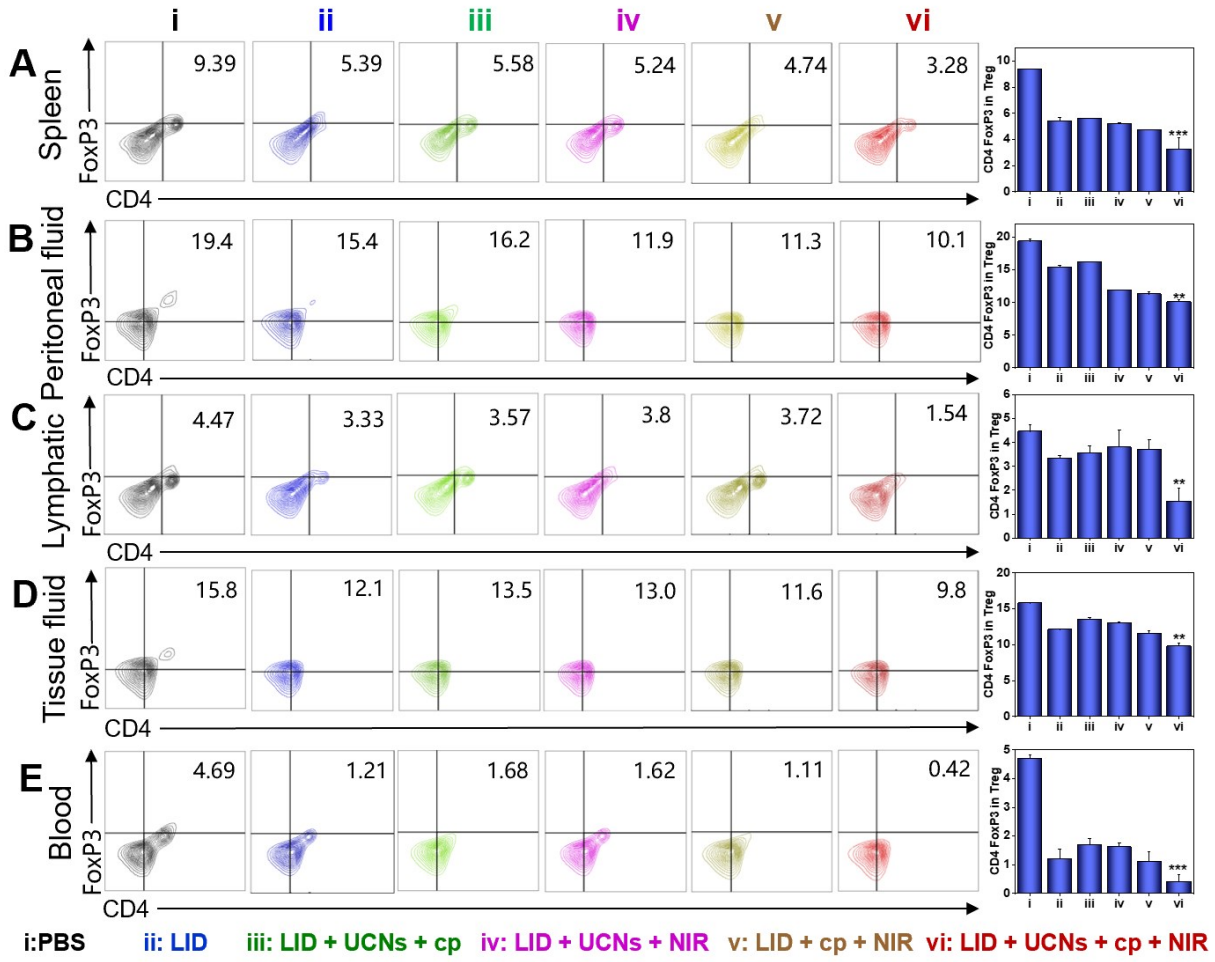

Fig. S25: Flow cytometry verified the number of Tregs in different organs of C57BL/6 mice. After the injection of LID, Tregs reduced in all organs of mice, and the number of Tregs was the least after the operation of engineering photosynthetic micro-nanodevice. A) Spleen. B) Peritoneal fluid. C) Lymphatic. D) Tissue fluid. E) Blood. Data represent mean ± D (n = 5); *P < 0.05, **P < 0.01 and ***P < 0.001 (one-way ANOVA).

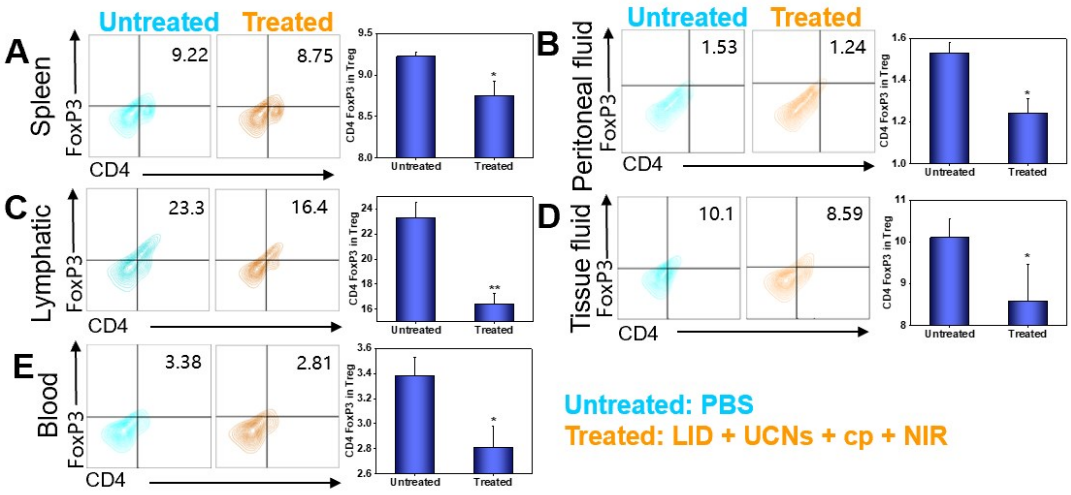

Fig. S26: Levels of Tregs in different organs of BALB/c mice. The Tregs reduced increased after engineering photosynthetic micro-nanodevice treatment. A) Spleen. B) Peritoneal fluid. C) Lymphatic. D) Tissue fluid. E) Blood. Data represent mean ± SD (n = 5); *P < 0.05, **P < 0.01 and ***P < 0.001 (one-way ANOVA).

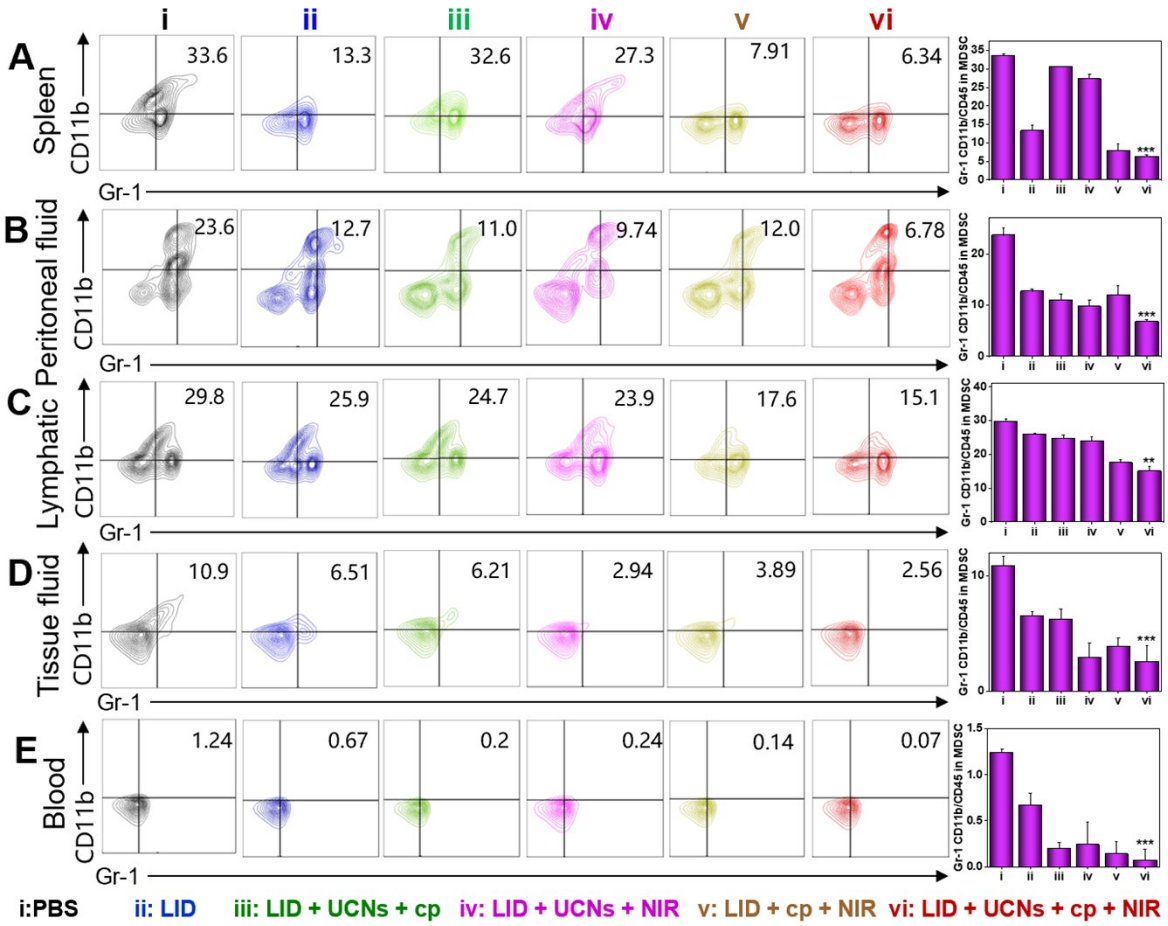

Fig. S27: Flow cytometry verified the number of MDSC cells in different organs of C57BL/6 mice. After the injection of LID, MDSC cells reduced in all organs of mice, and the number of MDSC cells was the least after the operation of engineering photosynthetic micro-nanodevice. A) Spleen. B) Peritoneal fluid. C) Lymphatic. D) Tissue fluid. E) Blood. Data represent mean ± D (n = 5); *P < 0.05, **P < 0.01 and ***P < 0.001 (one-way ANOVA).

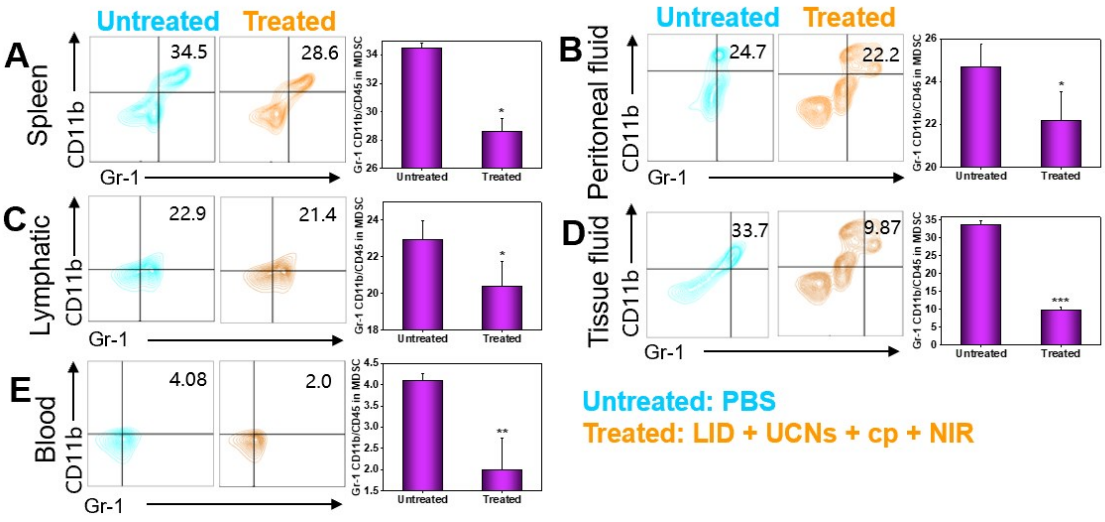

Fig. S28: Levels of MDSC cells in different organs of BALB/c mice. The MDSC cells reduced increased after engineering photosynthetic micro-nanodevice treatment. A) Spleen. B) Peritoneal fluid. C) Lymphatic. D) Tissue fluid. E) Blood. Data represent mean ± SD (n = 5); *P < 0.05, **P < 0.01 and ***P < 0.001 (one-way ANOVA).

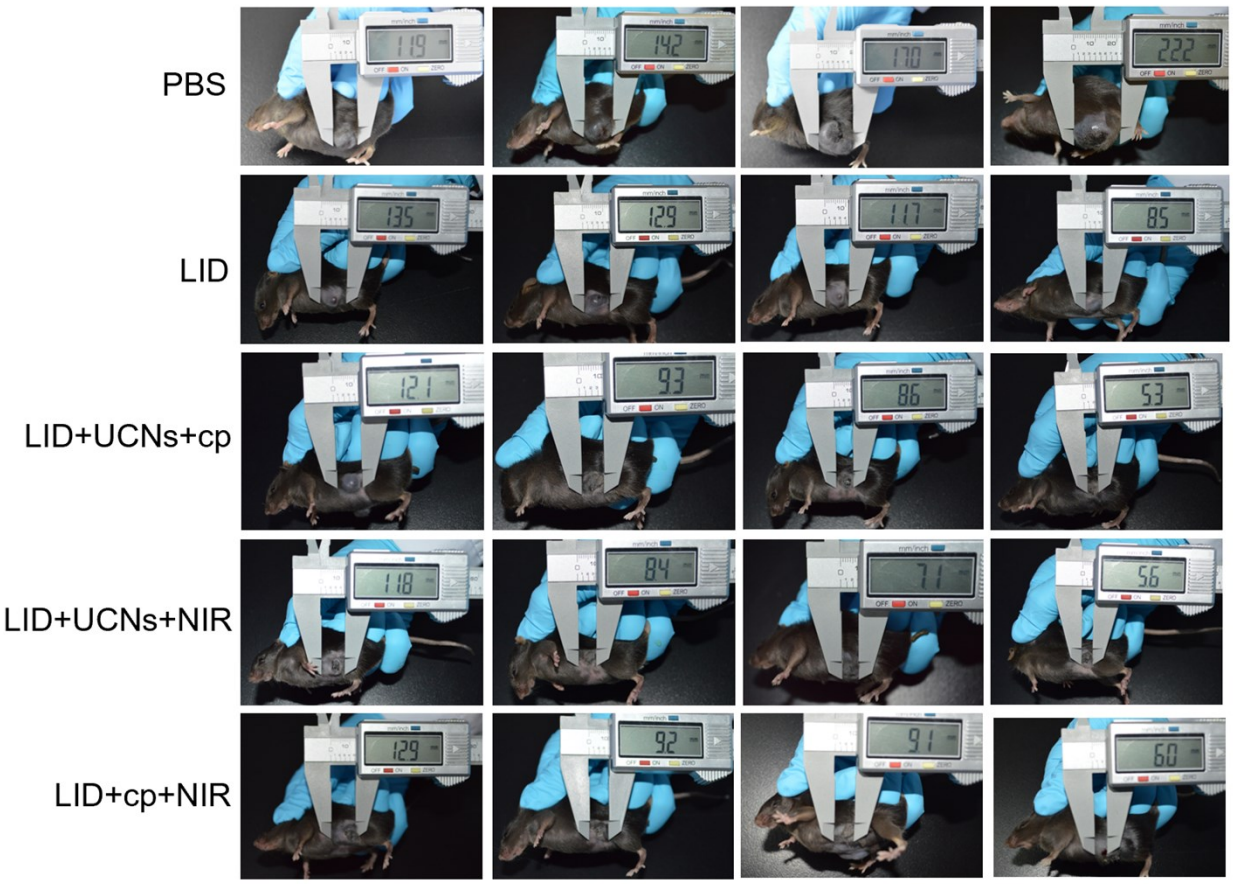

Fig. S29: The tumor size of each group changed after treatment. The above was the changes of tumor size in each group.

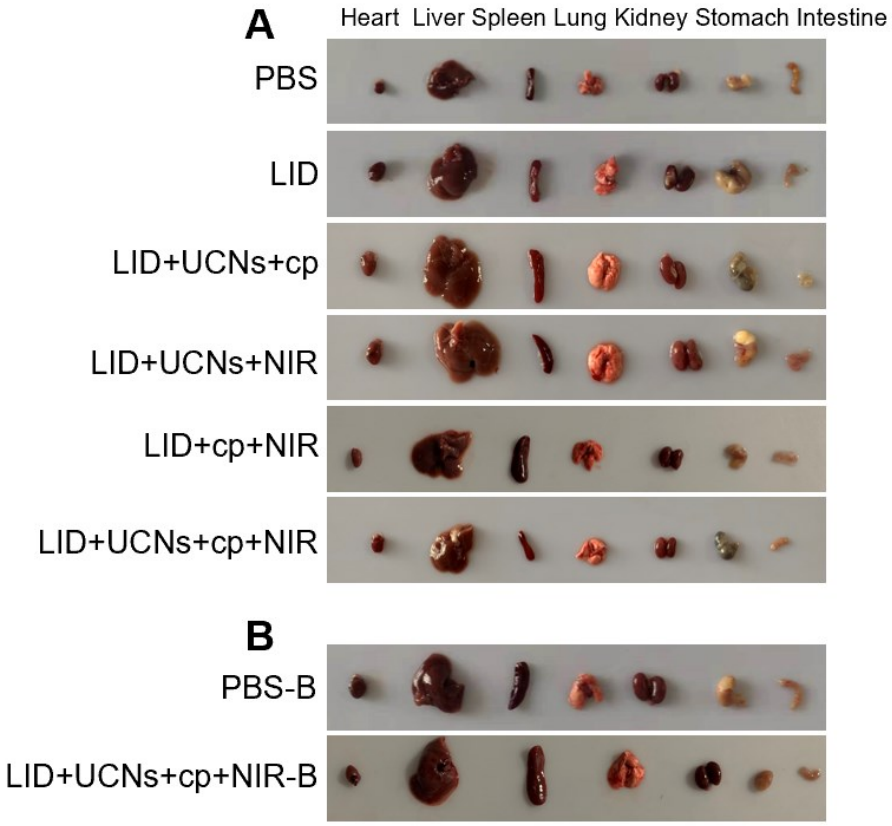

Fig. S30: Visceral was changed in each group. A） Visceral was changed in C57BL/6 mice. B) Visceral was changed in BALB/c mice. From front to back heart, liver, spleen, lung, kidney, stomach, intestine.

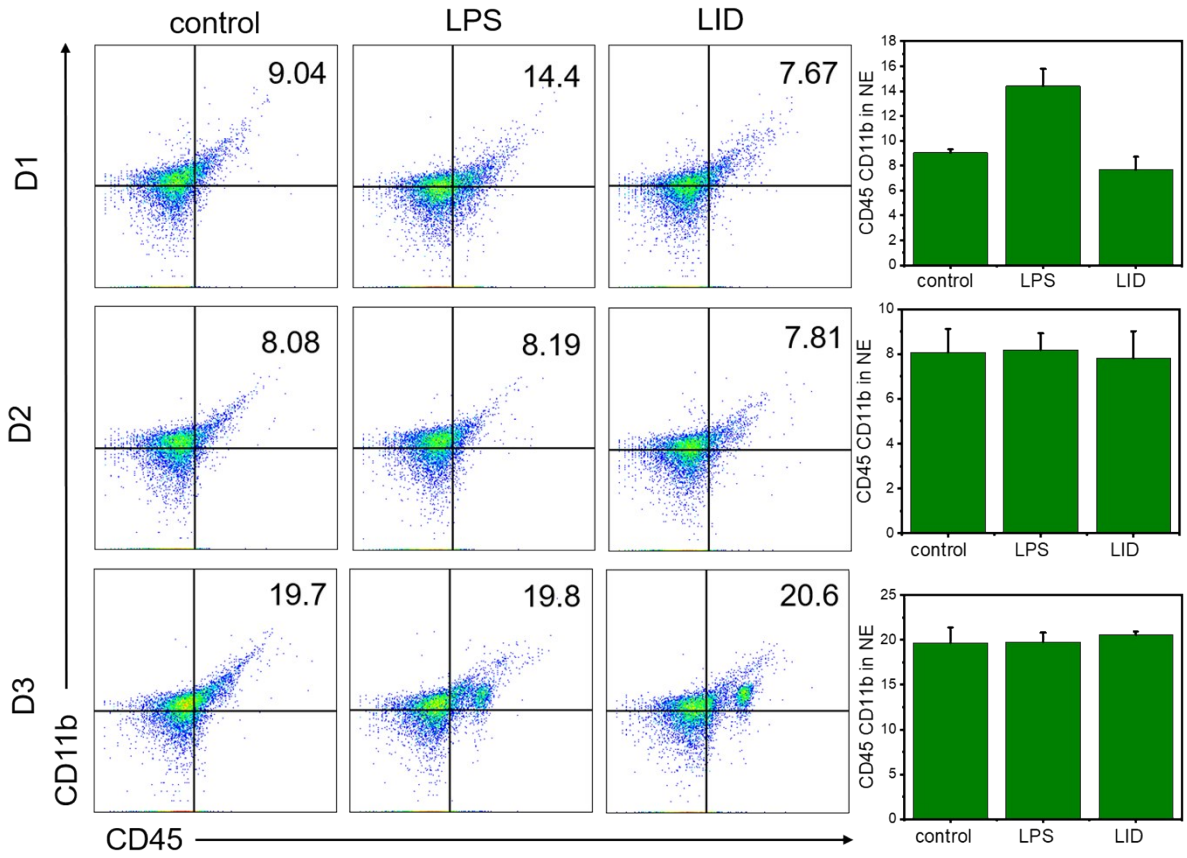

Fig. S31: Flow cytometry was used to detect the changes in neutrophil content at 1, 3, and 7 days after LPS and LID injection.

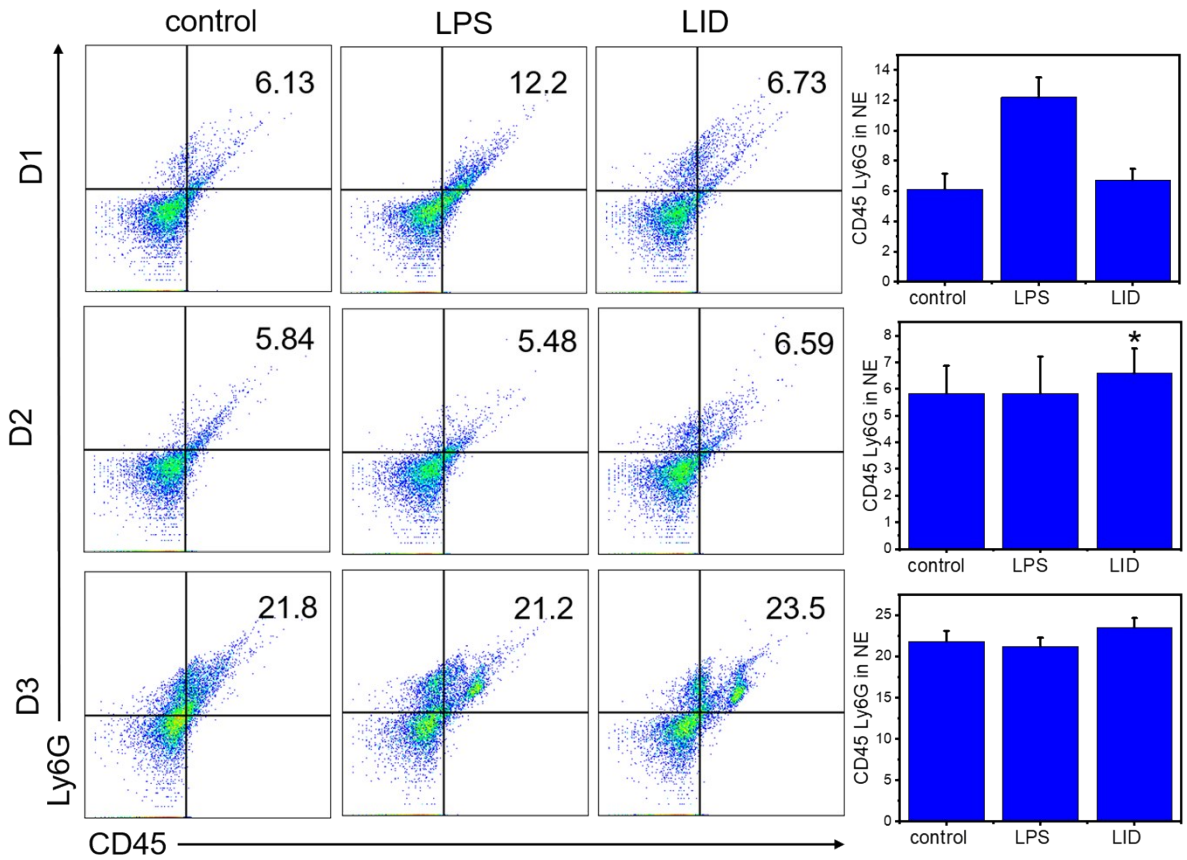

Fig. S32: Flow cytometry was used to detect the changes in monocyte content at 1, 3, and 7 days after LPS and LID injection.